Physics of the Earth and Planetary Interiors 283 (2018) 140–151

Contents lists available at ScienceDirect

Physics of the Earth and Planetary Interiors

journal homepage: www.elsevier.com/locate/pepi

The 1952 Kern County, California earthquake: A case study of issues in the analysis of historical intensity data for estimation of source parameters

Leah Salditch[a,*], Susan E. Hough[b], Seth Stein[a,c], Bruce D. Spencer[c,d], Edward M. Brooks[a,c], James S. Neely[a], Madeleine C. Lucas[a]

[a] Department of Earth and Planetary Sciences, Northwestern University, 2145 Sheridan Rd., Evanston, IL 60208, USA
[b] United States Geological Survey, 525 South Wilson Ave., Pasadena, CA 91106, USA
[c] Institute for Policy Research, Northwestern University, 2040 Sheridan Rd., Evanston, IL 60208, USA
[d] Department of Statistics, Northwestern University, 2006 Sheridan Rd., Evanston, IL 60208, USA

ARTICLE INFO

Keywords:
Earthquakes
Seismic intensity
Historic earthquakes
Seismic hazard

ABSTRACT

Seismic intensity data based on first-hand accounts of shaking give valuable insight into historical and early instrumental earthquakes. Comparing an observed intensity distribution to intensity-prediction models based on modern calibration events allows the magnitude to be estimated for many historic earthquakes. Magnitude estimates can also potentially be refined for earthquakes for which limited instrumental data are available. However, the complicated nature of macroseismic data and the methods used to collect and interpret the data introduce significant uncertainties. In this paper, we illustrate these challenges and possible solutions using the 1952 Kern County, California, earthquake as a case study. Published estimates of its magnitude vary from M_W 7.2–7.5, making it possibly the second largest in California during the 20th century. We considered over 1100 first-hand reports of shaking, supplemented with other data, and inferred the magnitude in several ways using intensity prediction equations, yielding a preferred intensity magnitude M_I 7.2 ± 0.2, where the uncertainty reflects our judgement. The revised intensity distribution reveals stronger shaking on the hanging wall, south of the surface expression of the White Wolf fault, than on the footwall. Characterizing the magnitude and shaking distribution of this early instrumental earthquake can help improve estimation of the seismic hazard of the region. Such reinterpreted intensities for historic earthquakes, combined with U.S. Geological Survey (USGS) Did You Feel It? data for more recent events, can be used to produce a uniform shaking dataset with which earthquake hazard map performance can be assessed.

1. Introduction

In this paper, we explore issues associated with analysis of seismic intensity data using the 21 July, 1952 Kern County, California, earthquake as a case study. Seismic intensity characterizes the level of earthquake shaking by human perceptions and effects on made-man structures and objects within them. The Modified Mercalli Intensity (MMI) scale introduced by Wood and Neumann (1931), based on earlier scales widely used previously in Europe (see Musson et al., 2010), has long been preferred in the U.S. by engineers and seismologists. Reports of earthquake shaking have been collected and assigned intensity levels by U.S. government agencies for over a century. From 1924 onward, postcard questionnaires were collected by the U.S. Coast and Geodetic Survey (USCGS), who left stacks of questionnaires with postmasters and employees of large companies to be completed by themselves and others in the community shortly after earthquakes (Byerly and Dyk, 1936). The questionnaires asked whether the respondents and those around them felt the earthquake, whether it frightened or awoke them, whether small objects on shelves shifted or overturned, whether large furniture was shifted, and whether and how buildings were damaged or destroyed. These questions correspond directly to indicators used in the MMI scale. Later, this information was collected via randomized telephone surveys and mailed postcards (Dewey et al., 1995). Presently, felt reports are collected online through the USGS Did You Feel It? (DYFI) website, making them easier to collect and interpret (Wald et al., 1999a). The DYFI system assigns numerical Community Internet Intensity (CII) values using a modification of the algorithm proposed by Dengler and Dewey (1998) to determine Community Decimal Intensities (CDI) from questionnaire responses. DYFI intensity values characterize representative shaking in an area, and hence differ

* Corresponding author.
E-mail address: leah@earth.northwestern.edu (L. Salditch).

https://doi.org/10.1016/j.pepi.2018.08.007
Received 27 April 2018; Received in revised form 14 August 2018; Accepted 19 August 2018
Available online 22 August 2018
0031-9201/

systematically from conventionally interpreted MMI data, which tend to be based on the most dramatic effects (Hough, 2013).

Uncertainties in intensity values arise from several sources. Human perceptions of and reactions to shaking vary with a person's physical sensitivity and disposition. Building age and construction quality, on which information is often unknown or unspecified in first-hand reports, influence the level of damage and perceived or felt shaking. Methods of intensity data collection as well as the distribution of population relative to the epicenter can introduce sampling biases. How questionnaires are phrased can impact the responses. Information about the location of a damage report varies, sometimes giving only a city name or approximate location. These issues introduce uncertainties into the intensity values assigned from the observations. Further uncertainties arise when intensity-prediction models describing the variation of intensity with distance from the fault are used to estimate the earthquake's magnitude.

Despite these limitations, intensity values are important for earthquake hazard assessment because they directly represent damage and because the length of macroseismic records often far exceeds that of the instrumental catalog (e.g., Ambraseys et al., 1983). For early instrumental and even recent earthquakes, intensity distributions can reveal the shaking distribution in far greater spatial detail than is possible using instrumental data. For historical earthquakes, macroseismic information is often the primary data available. Revisiting historic intensity data is worthwhile, because historically assigned intensities are often inflated by 0.5–2.0 intensity units relative to modern practice (Ambraseys, 1971, 1983; Hough and Page, 2011; Hough, 2013, 2014). Even following modern practice, conventional intensity assignments are inherently subjective, leading to differences of 0.5–1.0 intensity units for the same report by different interpreters (Hough and Page, 2011).

The Kern County earthquake was one of the largest in California during the 20th century. Some of the issues discussed in our study were noted at the time. Reports from the town of Tehachapi illustrate how historic or traditionally assigned intensities tend to be inflated. In 1952 its main street was lined with old, weakly cemented, unreinforced brick buildings that were highly susceptible to damage from shaking (Steinbrugge and Moran, 1954). Tehachapi (Fig. 1) is close to the end of the surface rupture furthest from the epicenter and therefore in the direction of rupture which focused energy towards the town (Richter, 1958). These effects likely account for the fact that many buildings downtown were damaged, causing most of the 12 fatalities that resulted from this earthquake, and extensive damage occurred to the Southern Pacific Railroad due to tunnel collapse and track warping. The shaking and damage made Tehachapi the focus of media coverage. Richter (1958) notes, "These deaths also focused the attention of the press, the public, and even of officials who should have been better informed, on the losses at Tehachapi disproportionately to those elsewhere," hinting at media's tendency to report the most dramatic stories rather than more representative effects. Richter also notes, "Many structures on the main street [of Tehachapi] were of this character [outdated masonry]; they showed such damage as caused incautious observers to rate the local intensity at VIII, though it is doubtful whether more than VII was actually indicated." In his seminal volume, Richter (1958) realized that intensity data for this earthquake were susceptible to inflation and would require careful interpretation keeping these influences in mind. In this spirit, we reinterpret intensity reports for this earthquake.

We refine the magnitude estimate and explore the associated uncertainties by reinterpreting over 1100 macroseismic intensity reports. These reports are cataloged in U.S. Coast and Geodetic Survey Abstracts of Earthquake Reports for the Pacific Coast and the Western Mountain Region, hereafter referred to as 'the primary dataset.' This refinement provides a new characterization of the shaking distribution of this early instrumental earthquake and a new estimate of its magnitude via recent intensity-prediction models.

2. The 1952 Kern County earthquake

On July 21, 1952 at 4:21 AM local time (GMT – 7 h) the White Wolf fault (WWF) ruptured in Kern County, California (Fig. 1). This earthquake illustrates that large earthquakes on secondary faults trending obliquely to the San Andreas fault, such as the WWF and the nearby and similarly-oriented Garlock fault, are important contributors to seismic hazard in California (Walls et al., 1998). The WWF is a steeply-dipping (up to 75°) reverse fault located east of the restraining bend in the southern portion of the San Andreas Fault (Bawden et al., 1997, 2001). It is thought to be slow-slipping, with long-term slip rate estimated at < 10 mm/yr, with variability throughout the Quaternary (Stein and Thatcher, 1981; Hearn et al., 2013). The Working Group for California Earthquake Probabilities (WGCEP, 2008) estimated a long-term slip rate of 0.23–1.55 mm/yr for different deformation models. Cutting the southern part of the San Joaquin Valley into the northern Maricopa subbasin and the southern Tejon Embayment, the WWF is blind from the epicenter of the 1952 mainshock at its southwest end to approximately the middle of the fault (Fig. 1). From there, the 1952 earthquake ruptured the surface to its northeastern endpoint, about 60 km from the epicenter. Bawden (2001) used geodetic data to develop a two-segment, right-stepping fault model with nearly uniform reverse slip of about 1.6–1.9 m and additionally up to 3.6 m of left-lateral slip in the epicentral patch. Stein and Thatcher (1981) developed a similar rupture model, with three fault segments whose dip gradually decreases away from the epicenter.

It has been hypothesized that this earthquake was triggered or induced by stress changes associated with oil production. The epicenter was within a few kilometers of an extraction well, shortly after production started from a deep (3 km) horizon (Hough et al., 2017). Although it is impossible to prove that the earthquake was induced by anthropogenic activity, it may have been one of the largest induced earthquakes (Foulger et al., 2017).

The Kern County earthquake was the most widely felt earthquake in California over the 50 years following the 1906 San Francisco earthquake. Although the 1952 earthquake was studied in detail at the time (Steinbrugge and Moran, 1954; Oakshotte, 1955; USDOC, 1966), as well as by later studies, estimates of its magnitude vary. The current USGS estimate is M_W 7.5 (Hutton et al., 2010). Instrumentally derived estimates include M_S 7.7 (Gutenberg and Richter, 1954; Richter, 1958), M_W 7.3/M_S 7.2 (Ben-Menahem, 1977), M_L 7.2 (Kanamori and Jennings, 1978), and M_S 7.8/m_B 7.3 (Abe, 1981). Bawden (2001) geodetically determined M_W 7.2. Bakun (2006) used 647 reinterpreted historic intensity assignments to estimate an intensity magnitude, a magnitude derived from intensity data, of M_I 7.3.

3. Reinterpretation of historic macroseismic intensity data

Over 1100 reports of shaking were compiled by the USCGS and assigned MMI intensities (USDOC, 1966). We compared the originally assigned intensity values with our reinterpretations of the same data. We augmented our reinterpreted intensity assignments with intensities derived from 12 strong motion data points, 67 retroactively-reported DYFI data points, 12 data points for damaged electrical transformers, and observations of precariously balanced rocks. Adding these data makes the reinterpreted dataset more robust, because many of the original intensity assignments close to the epicenter were based on geologic indicators such as rock slides, secondary ground deformation, and groundwater perturbations, which are now recognized to be unreliable indicators of shaking intensity (Ambraseys et al., 1983). About 7% of the primary dataset are based on such geologic indicators, which disproportionately controlled the highest intensity assignments in the original assessment. These descriptions were not considered in our reinterpretations. The primary dataset contains 1137 reports with historically assigned intensities that we refer to as original intensities. Our reinterpreted dataset (primary dataset minus reports describing

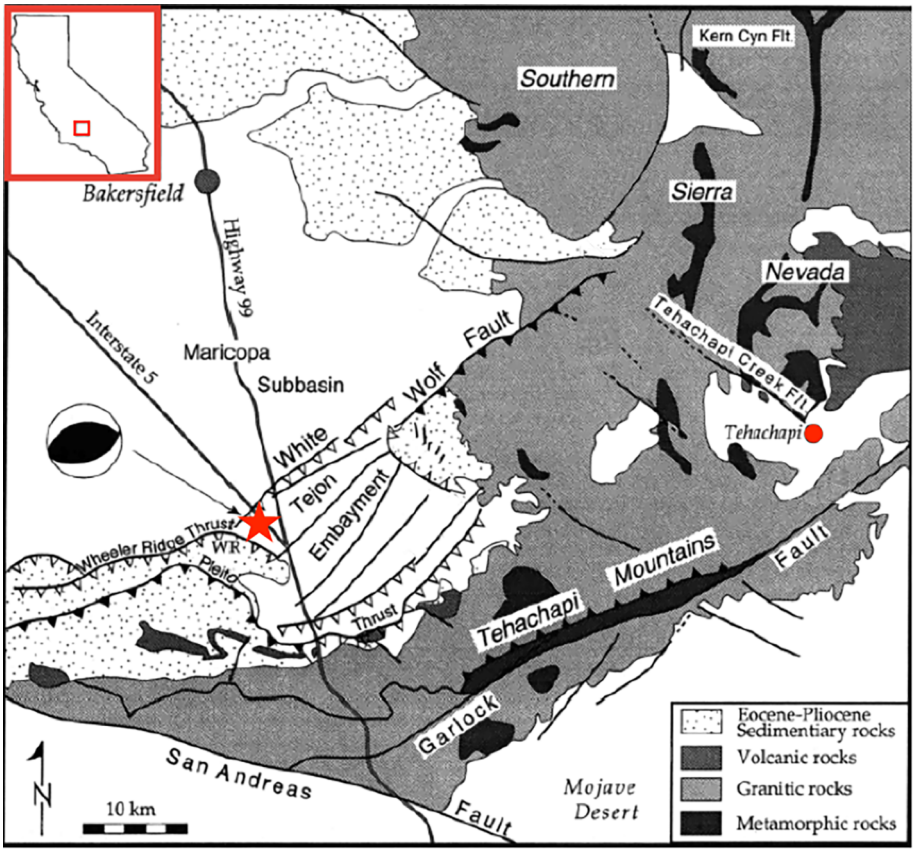

Fig. 1. Geology of the epicentral area. Open barbs represent blind thrusts, filled barbs represent exposed thrusts. Focal mechanism is 1952 mainshock, star indicates the epicenter. (After Bawden et al., 1997).

geologic/industrial effects plus additional data) contains 1144 reports, hereafter referred to as reinterpreted intensities.

Latitudes and longitudes for locations in the primary dataset, which mainly gives city names, come from the NOAA Earthquake Intensity Database. For locations where more detail is provided, for instance a street address or named electrical substation, latitude and longitude were found using Google Earth after confirming that street names and locations remained unchanged since 1952 by using USGS historical topographic maps (http://historicalmaps.arcgis.com/usgs/).

To explore the subjectivity of intensity assignments, we compared reinterpretations of the primary dataset made by two different analysts. This allows an evaluation of inter-rater variability and reliability. We compared intensity assignments only when both interpreters provided an assignment, i.e. excluding reports for which either interpreter was unable to assign an intensity based on the information given. 34% of assignments were identical between interpreters, 70% were within ± 0.5 MMI unit, and 97% were within ± 1 MMI unit. The absolute value of the mean difference between the interpreter's intensity assignments was 0.2 MMI units.

We also considered other sources of information that can constrain ground motions, including electrical transformer damage caused by the earthquake. The toppling of transformers has been investigated by earthquake engineers and can be related to Peak Ground Acceleration (PGA) via fragility curves, which can then be used to estimate MMI (Huo and Hwang, 1995). Detailed descriptions of transformer damage (Peers, 1955; USDOC, 1966) indicate how many transformers were toppled at a given substation. To estimate PGA, we compared the estimated percentage of overturned transformers to fragility data presented by Huo and Hwang (1995). Similarly, the preservation or overturn of precariously balanced rocks has been used to infer PGA and intensity at a number of locations in the near field (Brune et al., 2004).

We also considered peak ground acceleration data from 12 strong motion recordings of the earthquake (Murphy and Cloud, 1954). These data were recorded by instruments that operated in trigger mode, with no pre-event memory. For a large earthquake, these instruments generally triggered on the P wave and captured the full S wave. We converted PGA data to instrumental MMI using the relationship determined by Worden et al. (2012). Instrumental PGAs range from 1 to 25% g, corresponding to instrumental intensity values 3.3–7.2.

Table 1 gives examples to illustrate differences between original to reinterpreted MMI assignments. Our reinterpretation of felt reports differed from the original in the following ways:

1. Taking the Ambraseys et al. (1983) conservative approach to secondary geologic indicators.
2. Using quartile decimal (e.g. 5.0, 5.25, 5.5, etc.), rather than integer values of MMI.
3. Weighting our inferred intensities to give more weight to the disturbance of objects than to subjective human reactions. Originally, the disturbance of objects and personal reactions were given about equal weight for the lower MMI intensities (USDOC, 1966).
4. Assigning MMI 5 only when accounts describe toppling of small objects, a key objective indicator for this intensity level (Richter, 1958).
5. Rather than characterizing weakly felt intensities as a range of MMI 1–3, as was the earlier practice, we differentiated between MMI 2 and 3: MMI 2 for reports of "felt by few" without objective indicators, and MMI 3 for reports of "felt by many" accompanied by reports of hanging objects having swung.
6. Assigning MMI 1 for sites "Reported not felt", following Ambraseys et al. (1983) recommendation.

The reinterpreted intensity values are generally although not uniformly lower than originally inferred values (Figs. 2 and 3). The

Table 1
Example reports from primary dataset, comparing original and reinterpreted MMI. Groundwater and secondary geologic indicators were not considered in the reinterpretations.

Location	Report (edited slightly for space)	Original MMI	Reinterpreted MMI
Pleasant Grove, CA	Felt by several in community. One reported electric cord swung.	1–3	3
Carmel Valley, CA	Motion slow, lasted 30 s. Awakened many, frightened few, felt by some outdoors. Rattled windows, doors. Hanging objects swung.	5	4
Shell Beach, CA	The press reported a large bone fell off museum shelf.	6	6
Woody, CA	Motion rapid, rolling, lasted l minute. Felt by and awakened all in community, frightened many. Rattled windows, doors, dishes. Hanging objects swung. Trees, bushes shaken slightly. Shifted small objects. Overturned vases and small objects. Knickknacks, books, pictures fell. Broke dishes and vases. Water supply and springs milky.	7	5.5
Miracle Hot Springs, CA	Motion rapid, lasted 14 s. Felt by, awakened, and frightened all. Rattled windows, doors, and dishes; house creaked. Hanging objects swung N. Trees, bushes shaken strongly. Shifted small objects and furnishings; overturned vases, etc., small objects and furniture. Miracle Hot Springs went dry during the first shock, but resumed flow during the later shocks. Temperature of water seemed hotter. Many rock slides in canyon. Democrat Springs went completely dry.	8	6

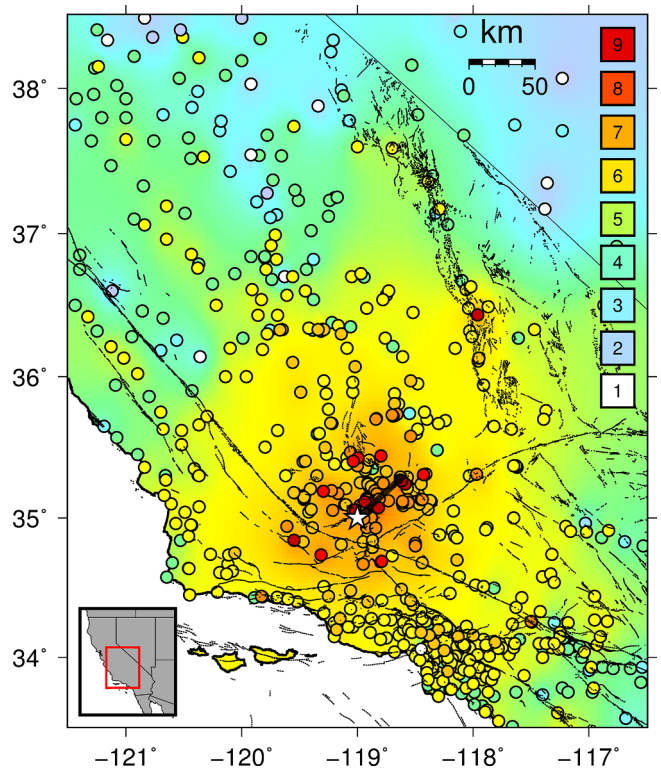

Fig. 2. Map of original intensity assignments. Circles show individual assignments, and the map is interpolated via continuous curvature splines from those points. Color scheme follows USGS Shakemap convention (Wald et al., 1999b). Thin lines are faults, thick line is 1952 WWF rupture. Star is epicenter.

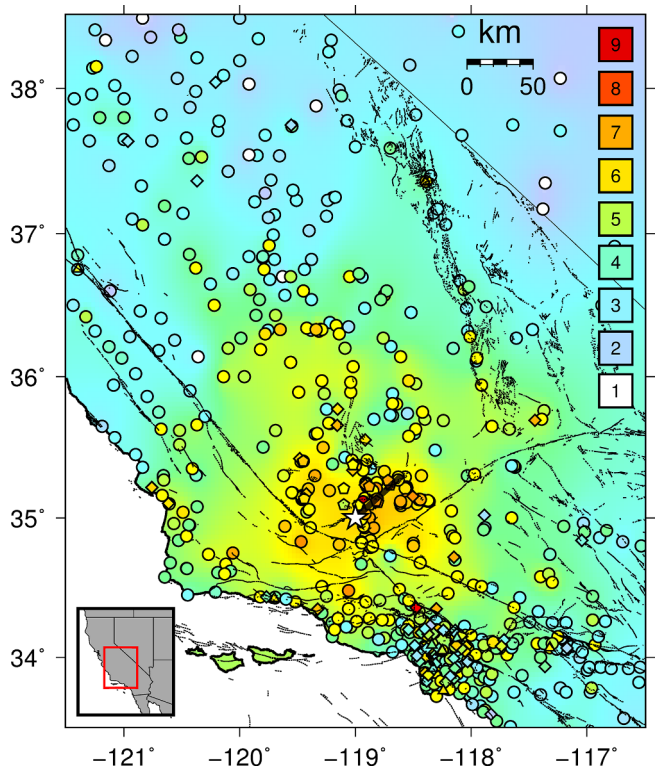

Fig. 3. Map of intensity assignments as reinterpreted in this study (circles). Also included are intensities derived from strong motion data (triangles), transformer/precariously balanced rocks (pentagons), and retroactively-reported DYFI (diamonds) — all consistent with reinterpreted values. Shapes show individual intensities, and the map is interpolated via continuous curvature splines from those points. Color scheme follows USGS Shakemap convention (Wald et al., 1999b). Thin lines are faults, thick line is 1952 WWF rupture. Star is epicenter.

absolute value of the mean difference between original and reinterpreted intensities is 0.6 MMI units. Some of this difference results from our assignment of quarter units rather than integral units. Reinterpretations are consistent with the retroactively-reported DYFI, instrumental, transformer and precariously balanced rock data (Fig. 3). Figs. 2–4 show locations of individual data points, with the remainder of the map interpolated through the 'surface' function of the Generic Mapping Tools, which grids data using adjustable tension continuous curvature splines (Wessel and Smith, 1991).

Based on their analysis of precariously balanced rock and toppled transformer observations, Brune et al. (2004) concluded that accelerations were higher on the hanging wall (southern side) of the WWF, in particular along the northeastern half of the rupture, where the rupture reached the surface (Fig. 1). They further concluded that along the southwestern half of the rupture, which they assume to have been blind, more significant energy was transferred to the footwall. Our reinterpreted intensity distribution also suggests that shaking was lower on the footwall and that intensities were lower along the southwest part of the foot wall as well, although this part of the intensity field is not well constrained (Fig. 4).

To further explore the distribution of shaking, we consider the distribution of residuals relative to an appropriate baseline. As discussed at length in the following section, it is not clear what the optimal baseline is for this event. We use the intensity prediction equation from Atkinson and Wald (2007), hereafter AW07, assuming intensity magnitude M_I 7.2, which is found by trial-and-error to provide a good average fit to the intensities (Fig. 5). Because of uncertainty about the appropriate baseline, the residuals illuminate differences in relative

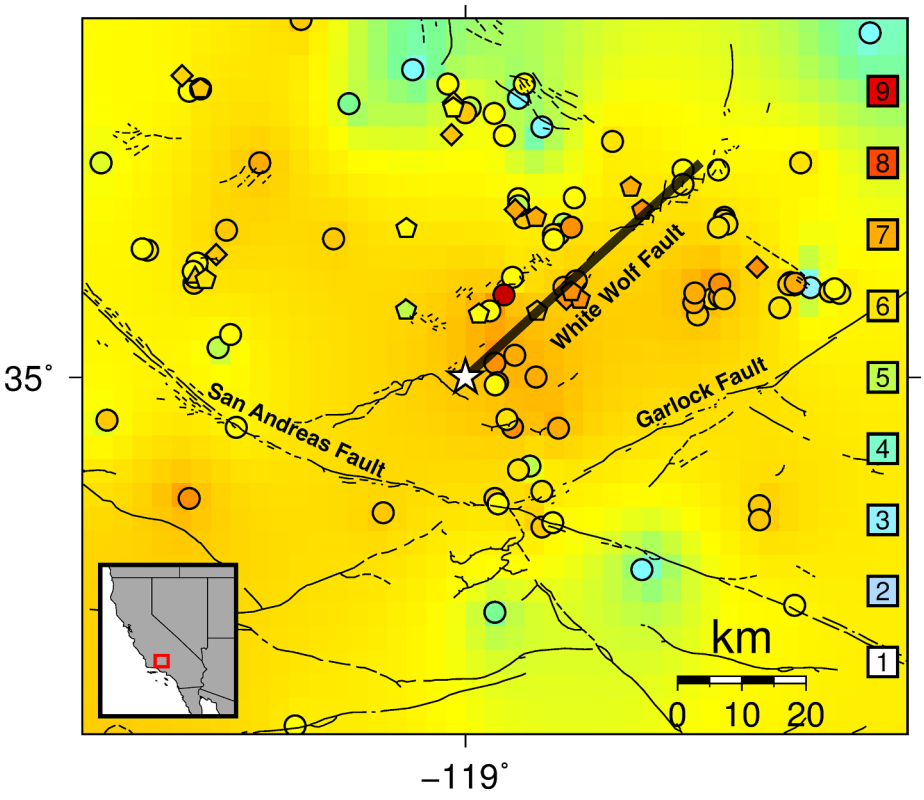

Fig. 4. Map of near-field intensities as reinterpreted in this study (circles). Also included are intensities derived from strong motion data (triangles), transformer/precariously balanced rocks (pentagons), and retroactively-reported DYFI (diamonds). Shapes show individual intensities, and the map is interpolated via continuous curvature splines from those points. Color scheme follows USGS Shakemap convention (Wald et al., 1999b). Thin lines are faults, thick line is 1952 WWF rupture. Star is epicenter. Higher intensities are observed on the hanging (southern) wall of the fault.

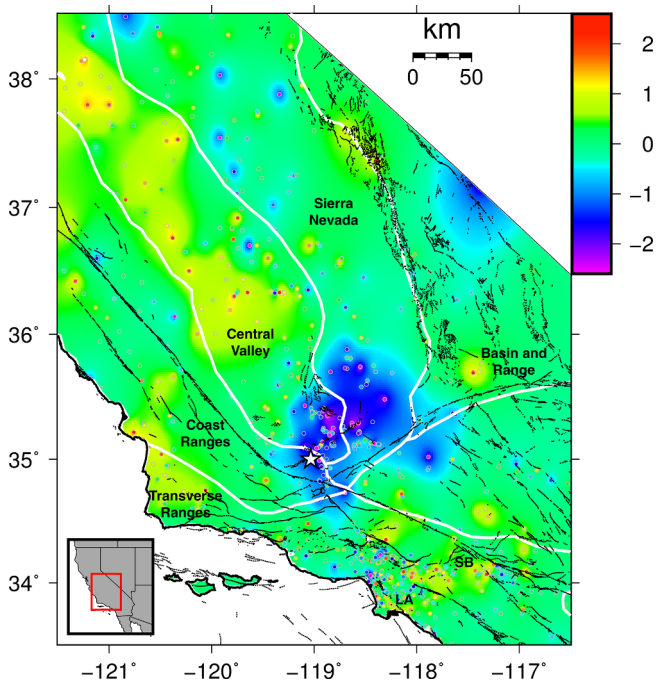

Fig. 5. Map of intensity residuals, relative to the AW07 IPE assuming an intensity magnitude of 7.2. Circles show individual points and the map is interpolated from those points. Residuals from Nevada are masked out due to sparse data available to constrain the interpolation there. Thin black lines are faults, white lines are major physiographic boundaries, star is epicenter of 1952 earthquake. SB is San Bernardino Basin, LA is Los Angeles Basin.

shaking severity, but not necessarily absolute amplification/deamplification. Fig. 5 reveals several first-order effects: 1) intensities are modestly elevated at some but not all sediment sites, including some sites in the Los Angeles and San Bernardino basins and in the Central Valley; 2) intensities are modestly elevated along a swath trending northwest through the Coast Ranges; 3) near field intensities are systematically low, in particular to the north of the fault trace. The amplification of shaking at sediment sites is an expected result (e.g., Borcherdt, 1970). Elevated shaking in the Coast Ranges is more enigmatic; we cannot propose an obvious explanation for this result, although it is possible that it reflects relatively low attenuation along paths to the west/southwest of the epicenter.

In the near-field, Fig. 5 suggests deamplification of shaking, by −0.5 to as much as −1.5 intensity units. We suggest that this result reflects two effects. First, as discussed above, and proposed by Brune et al. (2004), shaking was lower on the footwall than the hanging wall, all the more so because we have not assigned intensities to locations on the hanging wall where only secondary geologic effects were reported. Secondly, we suggest that near-field shaking was deamplified by a pervasively non-linear response of near-surface sediments. The zone of estimated deamplification is similar to that inferred in the Kathmandu Valley during the 2015 Gorkha, Nepal, earthquake (Adhikari et al., 2017). Our conclusion is also consistent with the qualitative conclusion of Trifunac (2003), who showed that near-field damage during the 1933 Long Beach, California, earthquake was deamplified in some near-field regions by pervasively non-linear response of soft, water-saturated sediments.

4. Intensity prediction equations

Intensity Prediction Equations (IPE) predict the decrease of shaking intensity with distance for an earthquake of a given magnitude. To estimate the magnitude of the Kern County earthquake, we compare published IPEs to the intensity values. These equations are empirically determined, so uncertainties in the data used to derive them cause uncertainty in the IPEs.

We first use an IPE from Bakun (2006), hereafter B06, who built upon the IPE of Bakun and Wentworth (1997) by developing coefficients for historic earthquakes in southern California based on traditionally assigned intensity data for 20th century M_W 5.0–7.1

earthquakes:

$$MMI_T(M_I, D) = C_0 + C_1 M_I - C_2 D - C_3 \log(D) \quad \text{(B06)}$$

where MMI_T is a traditionally assigned intensity, M_I is intensity magnitude, and D is distance from the epicenter in km. For southern California: $C_0 = 1.64 \pm 0.91$, $C_1 = 1.41 \pm 0.11$, $C_2 = 0.00526 \pm 0.00158$, $C_3 = 2.63 \pm 0.36$. The Kern County earthquake was not used to derive this relationship because it occurred prior to 1960 and the onset of modern and consistently calibrated instrumentation. Bakun (2006) used 647 reports from the 1952 Kern County earthquake and estimated its intensity magnitude as M_I 7.3.

We also used an IPE from Atkinson and Wald (2007). This relation is derived from modern DYFI data from California, so it might provide a better fit to our reinterpreted intensities. However, it may also not be fully appropriate for our data. Although conservatively reinterpreted, our data are still traditional intensity values determined from first-hand accounts. Hence they differ fundamentally from DYFI data in which intensities assigned from individual questionnaires are averaged within ZIP codes or geocoded cells. The AW07 relationship is:

$$MMI_{DYFI}(M, R) = d_1 + d_2(M-6) + d_3(M-6)^2 - d_4 \log(R) - d_5 R + d_6 B - d_7 M \log(R) \quad \text{(AW07)}$$

where M is moment magnitude; $R = (D^2 + h^2)^{1/2}$; D is distance from fault in km; h is effective depth, equal to 14 km for California; $B = 0$ for $R \le R_t$ and $B = \log(R/R_t)$ for $R > R_t$; R_t is the transition distance in the attenuation shape, $R_t = 30.0$ for California. For California $d_1 = 12.27 \pm 0.24$, $d_2 = 2.270$, $d_3 = 0.1304$, $d_4 = 1.30$, $d_5 = 0.0007070$, $d_6 = 1.95$, $d_7 = 0.577$.

B06 predicts higher intensities than AW07 for a given magnitude at distances less than approximately 400 km, and lower intensities at distances more than 400 km (Figs. 6 and 7) (Hough, 2013). Hough (2014) concluded that these differences likely reflect systematic bias in traditionally assigned intensities relative to DYFI intensities. Both IPEs predict negative intensities at distances greater than 400 km from the source for the lowest magnitude (M 6) tested in this study. The distance to a negative predicted intensity increases with increasing magnitude. For AW07, negative intensities occur over 200 km further from the source than B06 for the same magnitude. Following Hough (2014), sites at which B06 and AW07 predicted intensity values below 1.0 were set to 1.0, analogous to the assignment of MMI 1 for accounts of "Reported not Felt." Hough (2014) found B06 was a better fit (lower Root Mean Square misfit) than AW07 for historically assigned intensities. This is not surprising given that B06 was derived using traditionally assigned intensity data rather than the DYFI data to which AW07 was fit.

AW07 and B06 assume different earthquake source geometries and thus use different definitions for distance. AW07 defines D as distance from the closest point on the fault, whereas B06 assumes a point-source and calculates D as distance from the epicenter. For distance from closest point on fault calculations, we used a linear approximation of the WWF (Figs. 2–4) from the epicenter (35°, −119°) (for uncertainties, see discussion in the electronic supplement to (Hough et al., 2017)), to the approximate endpoint of surface rupture (35.3°, −118.6°). The B06 point-source assumption is less appropriate for large earthquakes, such as this one with its 60 km long fault, so we also considered a point-source at the approximate midpoint of the surface rupture. We prefer to compute B06 distances from the midpoint of surface rupture rather than the epicenter because of the unilateral rupture propagation from the epicenter toward the endpoint. Considering the midpoint of surface rupture shifts the point-source toward the region of the fault where radiated waves are stronger due to directivity and thus where intensities are predicted to be highest. The fault's endpoint and midpoint of surface rupture were estimated using Google Earth and the WWF

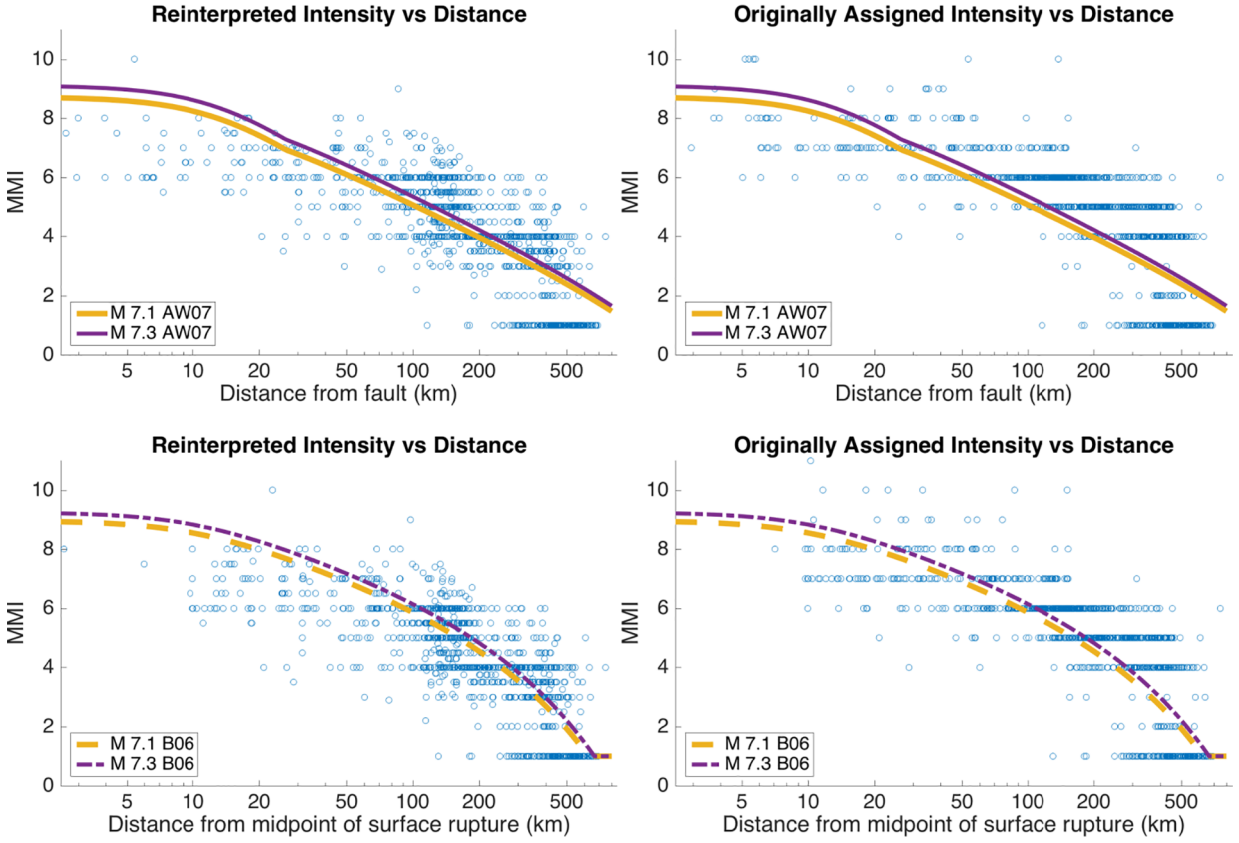

Fig. 6. Individual intensity assginments vs. $\log_{10}$ distance from (Top) nearest point on fault and (Bottom) approximate midpoint of surface rupture. (Left) Reinterpreted intensity assignments. (Right) Original intensity assignments. AW07 (solid lines) and B06 (dashed lines) predictions are shown for M 7.1 (thick lines) and M 7.3 (thin lines).

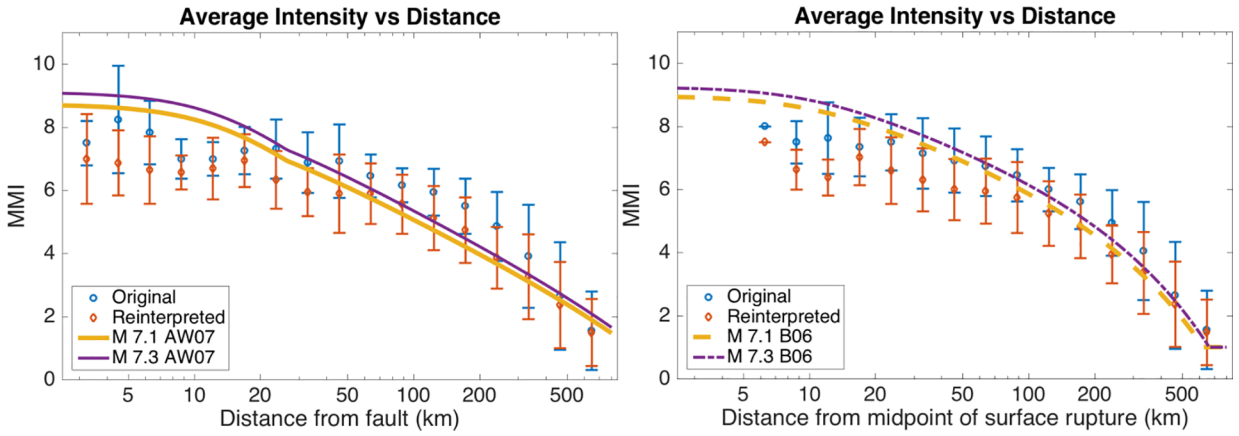

Fig. 7. Log_{10} bin averaged intensities ± one standard deviation, with IPEs for magnitudes M 7.1 and M 7.3. AW07 (left) computed using distance from closest point on the fault. B06 (right) computed using distance from approximate midpoint of surface rupture.

trace in the USGS Quaternary fault and fold database. The effects of these different definitions for distance are explored below.

5. Fitting intensity data

To estimate the magnitude of the earthquake from the intensity data, we computed the Root Mean Square (RMS) misfit between intensity assignments, either original or reinterpreted, with those predicted by the two IPEs for a range of magnitudes (Figs. 6–8). RMS was determined point by point: for every observation i, we predicted MMI at distance d_i, where d_i = distance in km from the source. RMS misfit is often illustrated graphically with spatial bin-averages of intensity (Fig. 7). However, using bin-averaged data decreased the best fit magnitude by 0.2–0.4 magnitude units compared to the full dataset. We prefer the point by point RMS analysis because it utilizes more information per point.

RMS misfit is defined as:

$$RMS(M_j) = \sqrt{\sum_{i=1}^{N} (\hat{y}_i - y_i)^2 / N}$$

where

M_j from 6.0 to 8.3 are earthquake magnitudes
y_i is MMI of observation i, either originally assigned or reinterpreted
$\hat{y}_i$ is expected MMI at d_i based on either IPE for the assumed M_j
N = total number of observations, 1144 for reinterpretations and 1137 for originals

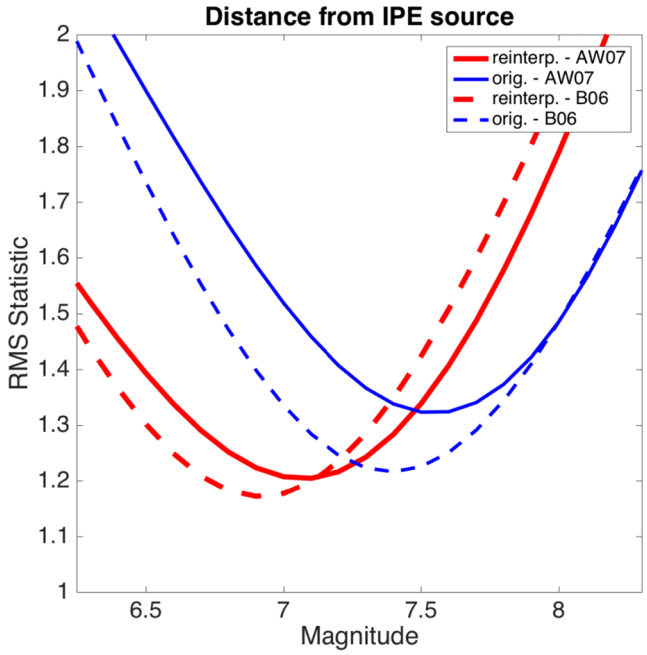

Fig. 8. RMS misfit between IPEs and reinterpreted or original intensity assignments for a range of magnitudes, computed as distance from closest point on fault for AW07, and from approximate midpoint of surface rupture for B06. The minimum misfit gives M_{best}. Thin lines are original intensity assignments; thick lines are reinterpreted. Solid lines are for AW07; dashed are for B06.

The minimum RMS over the range of magnitudes gives the best fit magnitude, M_{best} (Fig. 8, Table 2). This method uses the central value of the coefficients in B06 and AW07, and thus ignores the uncertainty in the IPE coefficients.

Calculating distances from the closest point on the fault yields a slightly lower M_{best} across all IPE-data pairs compared to the two point-source distances, differing by up to 0.2 magnitude units (Table 2). This occurs because many of the highest intensity observations are shifted closer to the fault, where intensities are expected to be highest. However, both AW07 and B06 still overpredict MMI at distances less than 20 km from the source, regardless of how distance is defined (Fig. 6). The final column of Table 2 considers a mixture of estimates, from closest point on fault for AW07 and from the approximate midpoint of surface rupture for B06. This mixed-source method, which we refer to as "IPE source," is our preferred combination.

Fig. 8 illustrates the effect of the choice of IPEs and of reinterpreting the data. Reinterpretation decreased the estimated magnitude by 0.4–0.5 magnitude units, reflecting our more conservative assessment of the data compared to the original interpretations. Differences between the IPEs result in a difference of 0.1–0.3 magnitude units for either dataset, with AW07 M_{best} magnitudes always higher than B06. This occurs because AW07 predicts lower shaking than B06 for a given magnitude (Figs. 6 and 7). Hence, to best fit a set of data, AW07 requires a higher magnitude than B06.

The B06 relationship provides the best fit, i.e. lowest minimum RMS over all magnitudes, for both reinterpretations and originally assigned intensities. For reinterpretations, the minimum RMS over all magnitudes only improves slightly from AW07 to B06. This suggests that AW07 is almost as good a predictor as B06 for these data, and potentially for other large historical earthquakes, if the intensities are interpreted carefully, following modern practices, and if sufficient macroseismic information is available to characterize the intensity distribution in detail.

This result appears to be counter to that found by Hough (2014) when analyzing the 1868 Hayward fault intensities as reinterpreted by Boatwright and Bundock (2008a), where B06 fit the reinterpreted

Table 2
Magnitude, M_{best}, inferred from minimum RMS for the different data-IPE pairs. M_{best} = M(min(RMS)) is assessed for distances computed from the epicenter, from the approximate midpoint of surface rupture, from the closest point on the fault, and using distances calculated with respect to the IPE definition (i.e. from closest point on fault for AW07 and from approximate midpoint of surface rupture for B06).

IPE – Data pair	M_{best} from epicenter	M_{best} from midpoint	M_{best} from closest point on fault	M_{best} from IPE source
AW07 – Reinterpreted	7.3	7.2	7.1	7.1
AW07 – Original	7.7	7.7	7.5	7.5
B06 – Reinterpreted	7.0	6.9	6.8	6.9
B06 – Original	7.4	7.4	7.3	7.4
Average	7.4	7.3	7.2	7.2

historic intensity data significantly better than AW07. Hough (2014) found the RMS to be nearly twice as large for AW07 for a given magnitude. We find considerably better agreement between the minimum RMS values of AW07 and B06 with reinterpreted intensity data for our preferred magnitude of the Kern County earthquake (Fig. 8).

The difference in which IPE best fits reinterpreted intensity data may be due to the fact that the 1868 Hayward intensity dataset reinterpreted by Boatwright and Bundock (2008a) only had ~160 reports, whereas the 1952 Kern County dataset is more than seven times larger. The increased number of observations decreases spatial sampling biases. We find M_{best} is 6.9–7.0 using the B06 IPE with point sources and reinterpreted data, which is lower than the M_I 7.3 that Bakun (2006) obtained with the same method from 647 intensities for the Kern County earthquake using distances calculated from the epicenter.

6. Uncertainties in M_{best}

How to address uncertainties in the IPEs and hence their suggested M_{best} is a challenge that we approached in several ways. Addressing uncertainties in IPEs requires some assumption about correlations because the correlations between pairs of coefficients in B06 and AW07 are not available. One approach is to entertain the extreme assumption that the uncertainties in the coefficients, represented by the associated ± values, have a correlation of 1, i.e. that the errors all move together in the same direction. In this perfectly correlated errors method, consideration of the errors takes the form of a simple upper/lower bound method by creating an upper and lower IPE for a given magnitude based on the upper and lower range of the coefficients. We then fit the data to the upper and lower IPEs. The M_{best} magnitudes of the minimized RMS for the upper and lower IPEs form the uncertainty ranges for the M_{best} of the central minimized RMS. AW07 provides an error range for only one of its coefficients, whereas B06 provides errors for all coefficients. Hence, the perfectly correlated errors method results in B06 having an apparently larger uncertainty than AW07 (Table 3, Fig. 9). In fact, using this method results in B06's M_{best} uncertainty spanning the entire range of magnitudes tested (6.0–8.3). Due to the difference in the number of coefficients with reported uncertainties between the IPEs, this method is not preferred.

Another approach is to assume that the errors of the IPE coefficients are all uncorrelated. We define δ_i as the uncertainty for coefficient C_i, $i = 0,\ldots,3$. For B06, the approximate standard deviation is:

$$SD(MMI_{B06}) = \frac{1}{2}\sqrt{\delta_0{}^2 + (\delta_1 M)^2 + (\delta_2 D)^2 + (\delta_3 \log(D))^2}$$

AW07 only provides an uncertainty for one coefficient, so if the other uncertainties are negligible the approximate standard deviation is:

$$SD(MMI_{AW07}) = \frac{\delta_1}{2}$$

(Use of the factor of ½ is based on interpretation of the reported ± amounts as 2 standard deviations). Using these values, we again apply a simple upper/lower bound method to the IPEs. The upper IPE for a given magnitude is the central IPE with one standard deviation added, whereas the lower IPE has one standard deviation subtracted (Fig. 9). The results are summarized in Table 3. Like the perfectly correlated errors method, this uncorrelated errors method uses an arbitrary assumption of constant correlation and is influenced by the different numbers of coefficients with reported errors between the IPEs. Thus, the uncorrelated errors method is also not preferred.

An alternative approach involved assessing the uncertainty in M_{best} by estimating its variance with a jackknife method (Shao and Tu, 1995). A jackknife approach involves repeatedly computing the desired statistic by leaving out a different subset of the data each time. This method views the data points as coming from a random sample and takes the coefficients in the IPEs as given (and nonrandom). This method has the advantage of not being influenced by the different number of coefficients in the IPE for which uncertainties were reported. We explored two different jackknife approaches, using simple random samples and spatially clustered samples. With a simple random sample approach, each record in the dataset was assigned a random number uniformly distributed between 0 and 1. To make the two datasets evenly divisible by 100, we took a simple random sample of 1100 observations selected without replacement from each. The data were sorted by the random numbers in ascending order, and the 1100 observations were formed into 11 groups of 100 observations (i.e. group 1 is records 1–100, group 2 is records 101–200, etc.). Each of the 11 groups is thus a non-overlapping simple random subsample of size 100. Using smaller subsample sizes than 100 led to subsample values of M_{best} that had zero variability. We then repeatedly compute M_{best} for each jackknife replicate sample of 1000 observations, formed by leaving out successive groups individually.

Spatial correlations are evident in the residual plot (Fig. 5). To account for this, we also use a spatial cluster sampling jackknife. The

Table 3
Uncertainty ranges (± SE) of best fit magnitude from different methods for distances calculated in the same manner as the respective IPE when derived (i.e. from closest point on fault for AW07 and from approximate midpoint of surface rupture for B06). This table is summarized in Fig. 10.

IPE – Data pair	Perfectly Correlated Errors	Uncorrelated Errors	Random Sample Jackknife	100 km^2 Spatial Jackknife	Standard Deviation of Residuals
AW07-Reinterpreted	6.9–7.2	7.0–7.2	7.0–7.2	6.9–7.3	6.5–7.8
AW07 –Original	7.4–7.7	7.5–7.6	7.3–7.7	7.1–7.9	6.9–8.3
B06 –Reinterpreted	6.0–8.3	6.4–7.5	6.8–7.0	6.8–7.0	6.5–7.4
B06 –Original	6.0–8.3	6.9–7.9	7.1–7.7	7.3–7.5	7.0–7.8

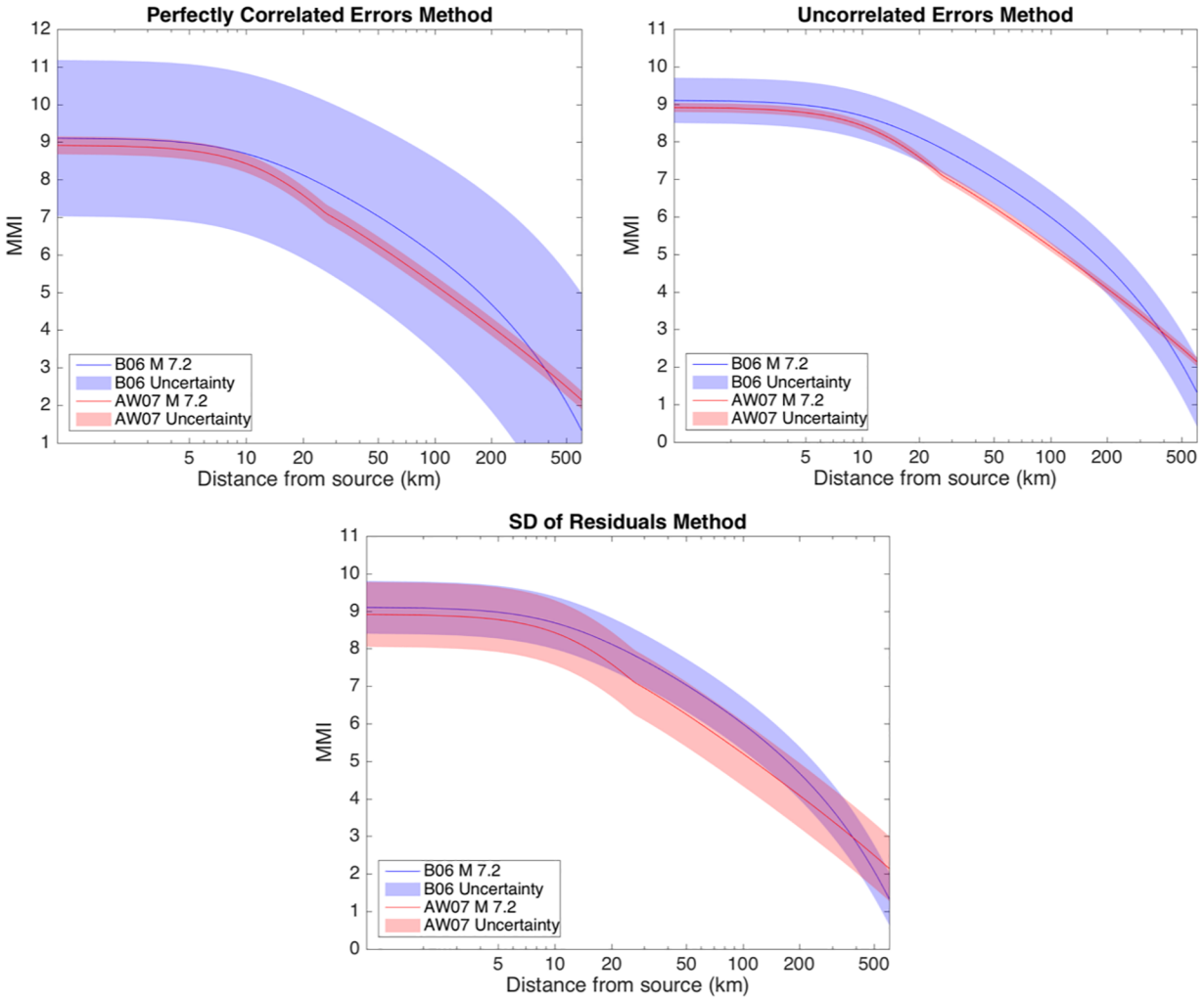

Fig. 9. Uncertainty of AW07 and B06 MMI with distance for M 7.2 predictions from: (top, left) perfectly correlated errors method; (top, right) uncorrelated errors method; (bottom) standard deviation (SD) of residuals method, which shows SD for the IPEs with respect to the reinterpreted intensities. Top row methods are influenced by the different number of coefficients with errors provided in the two IPEs, while bottom row is unaffected by this and thus preferred.

study area was spatially gridded into 100 km^2 blocks, which we treated as arising from cluster sampling. This resulted in 68 blocks with at least one observation. For the original dataset, the maximum number of observations in a block was 135, the median was 8, and the mean was 16.5. For the reinterpreted dataset, the maximum number of observations in a block was 168, the median was 8.5, and the mean was 16.8. We then computed M_{best} by excluding successive blocks of data individually. We did not include blocks with zero observations in the jackknife.

The jackknife sample excluding the jth group or block yields an estimate of M_{best}, $\hat{\theta}_{(j)}$. Combined, they yield $\hat{\theta}_{(.)} = \frac{1}{g}\sum_{j=1}^{g}\hat{\theta}_{(j)}$, where g is the number of groups for the simple random sample approach, and the number of blocks that contain at least one data point for the spatial clustering approach. The jackknife estimate of variance is $\hat{V}_{jack} = \frac{g-1}{g}\sum_{j=1}^{g}(\hat{\theta}_{(j)}-\hat{\theta}_{(.)})^2$, and the estimate of standard error (SE) is $SE = \sqrt{\hat{V}_{jack}}$. The resulting uncertainties are given by the range of $M_{best} \pm SE$ (Table 3).

A final measure of uncertainty comes from the standard deviation of residuals, defined as observed minus predicted MMI, for the different data-IPE pairs. Atkinson and Wald (2007) used this method on the mean MMI of $\log_{10}$ distance binned observations (as in Fig. 7) and found that their model had an uncertainty of 0.4 MMI units. We followed suit and found the standard deviation of residuals for the different data-IPE pairs. Using distances from IPE source, the standard deviations of the residuals computed at the IPE-data pairs respective M_{best} ranged from 0.6 for B06 – Original to 1.0 for AW07 – Original. As done above, we created an upper and lower IPE by adding or subtracting the resulting standard deviation from the central IPE for a given magnitude (Fig. 9). We then fit the full datasets to the upper and lower IPEs, giving a range of M_{best}. Results are summarized in Table 3. This method, like the two jackknife methods, is not affected by the number of coefficients with errors provided in the different IPEs. Of the three preferred methods, the standard deviation of residuals yielded the largest estimate of uncertainty in M_{best}.

7. Results

As discussed previously, it is likely that neither the AW07 nor the B06 IPE is entirely appropriate for a reinterpreted traditional intensity dataset like that determined in this study. From the results in Tables 2 and 3, which are summarized in Fig. 10, the plausible range in M_{best} values is 6.5–7.8. This range encompasses those for reinterpreted data from B06 and AW07 via the two jackknife and standard deviation of residuals methods. Fig. 10 shows the uncertainty ranges from Table 3 and a combined sum of the number of occurrences of specific magnitudes within these ranges. The combined sum yields a well-defined peak at M 7.1 for distances computed with respect to the IPE source.

The AW07 relationship was not expected to be a good predictor of originally assigned intensities, so this pair's outlier status for minimum

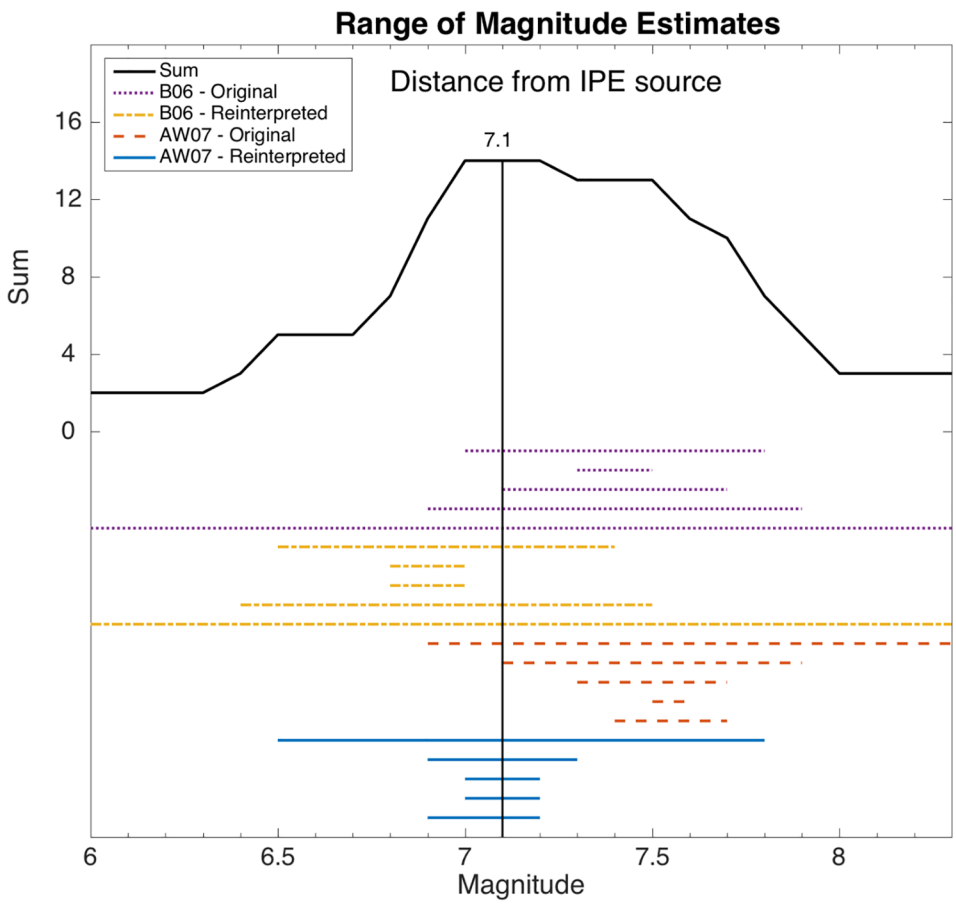

Fig. 10. Range of M_{best} magnitude estimates from the five uncertainty methods for the four IPE-data pairs (Table 3), computed as distance from closest point on the fault for AW07, and from approximate midpoint of surface rupture for B06. The sum line is the sum of the occurrences of a given magnitude, showing a peak at centered on M 7.1.

RMS misfit and corresponding M_{best} is not surprising. To explore the influence of this outlier, we considered the IPE-data pairs with and without AW07 – original. The variance of the RMS among the four IPE-data combinations is minimized at M 7.4 with respect to the IPE source, whereas the variance is minimized at M 7.2 when the outlier is excluded.

An unweighted average of M_{best} over all four IPE-data pairs gives M 7.2 when distance is computed from IPE source (Table 2). An unweighted average of M_{best} using the three more consistent IPE – data pairs (i.e. excluding AW07 – original) gives M 7.1 for distances computed from IPE source.

Using inverse-variance weighting, we estimate a combined-best magnitude for each uncertainty method considering all four IPE-data pairs and considering the three consistent pairs, i.e. excluding AW07 – original. Using weights designed to capitalize on small uncertainties, the inverse-variance weighting method is:

$$\widehat{M} = \sum_{i=1}^{n} \frac{M_i}{\varepsilon_i^2} \Big/ \sum_{i=1}^{n} \frac{1}{\varepsilon_i^2}$$

where

$\widehat{M}$ is the combined-best magnitude estimate
i is the IPE-data combination
n is the number of IPE-data pairs considered, in this study 3 or 4
M_i is M_{best} for combination i, from Table 2
ε_i is the uncertainty range of M_{best} for combination i, i.e. the ranges from Table 3

Results of this analysis are summarized in Table 4. The unweighted average of all four IPE-data pairs is the same as the average inverse-variance weighted M_{best} of all four pairs over the five different uncertainty methods.

Based on these results, which give single points, and those summarized in Table 3 and Fig. 10, which give ranges, our best estimate of the magnitude of the Kern County earthquake is M_I 7.2 ± 0.2. Recall that intensity magnitude M_I, a magnitude obtained from intensity data, is derived in terms of moment magnitude M_W and so is designed to reflect the moment magnitude. Because it is not a moment magnitude in the strictest sense, we prefer the M_I terminology. The reported uncertainty of ± 0.2 reflects the collective (and consensus) judgement of the authors, based on our uncertainty analyses, that the odds are 2:1 that the true M_I is in the range 7.0–7.4.

In this study, AW07 combined with reinterpreted intensity data using distances computed from the closest point on the fault gives M_{best} that agrees most closely with this preferred magnitude. Hence, we conclude that AW07 best describes the reinterpreted shaking distribution of the 1952 Kern County earthquake.

8. Discussion

The different methods presented to infer the uncertainty in M_{best} are sensitive to different aspects of the underlying uncertainties in both the IPEs and the data. The perfectly correlated and uncorrelated error methods account only for uncertainties in the IPEs. The jackknife methods account for sampling errors under assumed hypothetical sampling models. The spatial jackknife additionally takes spatial correlation of data into account. The standard deviation of residuals method is sensitive to both the IPE and, to some extent, the data

Table 4
Results of inverse-variance weighting for the different uncertainty methods, with the average over all methods, using distances calculated in the same manner as the respective IPE when derived (i.e. from closest point on fault for AW07 and from approximate midpoint of surface rupture for B06). Inverse-variance is computed using the three IPE-data pairs with the lowest minimum RMS values (inverse-variance 3) and with all four IPE-data pairs (inverse-variance 4).

IPE – Data Pair	Perfectly Correlated Errors	Uncorrelated Errors	Random Sample Jackknife	100 km^2 Jackknife	Standard Deviation of Residuals	Av.
Inverse -variance 3	7.1	7.1	7.0	7.1	7.2	7.1
Inverse -variance 4	7.3	7.4	7.1	7.2	7.2	7.2

sampling. The distance-binning of the residuals method takes some spatial correlation into account, although not to the extent that the spatial jackknife method does, while also considering lack of fit of the data to the IPE.

Although questions remain about the consistency of DYFI intensities and traditional intensities assigned following modern practices (Hough, 2013, 2014), we believe that our reinterpretation of historic intensity data for the Kern County earthquake provides an improved characterization of both its magnitude and the ground shaking. Our preferred magnitude estimate is slightly lower than the current catalog estimate (Mw 7.5; Hutton et al., 2010) but consistent with the geodetically determined magnitude (Mw 7.2; Bawden, 2001) and the previously determined intensity magnitude (M_I 7.3; Bakun, 2006). The earthquake generated potentially damaging ground motions (MMI 6–7) to distances of over 300 km, with an overall felt extent covering most of California. Our results suggest that shaking was stronger on the hanging (south) wall of the White Wolf fault than on the footwall, a fortuitous result because most of the population in the near-field region was north of the fault.

A growing body of evidence further suggests that near-field shaking in large earthquakes can be significantly tempered by pervasively nonlinear response of soft, water-saturated sediments (e.g., Trifunac, 2003; Adhikari et al., 2017). Non-linear effects pose a potential challenge for the development of intensity prediction equations, in particular if they are not well constrained for large magnitudes. Hence extrapolations that are reasonable for relatively weak shaking levels might not be appropriate at the strongest near-field shaking levels. A further practical caution, however, is that the extent of deamplification will depend on the impedance and degree of water saturation of near-surface sediments. As discussed by Trifunac (2003), non-linear effects will be less pronounced on older, more consolidated sediments than on soft, water-saturated sediments.

Our reinterpreted intensity distribution provides a missing puzzle piece for the larger picture of California's maximum historically observed earthquake intensities. Other big pieces are already in place: intensities have been revisited in recent years for the large events of Fort Tejon in 1857, Hayward in 1868, Owens Valley in 1872, Laguna Salada in 1892, San Francisco in 1906, and Santa Barbara in 1925, as well as many moderate historic events (Meltzner and Wald, 1999; Martindale and Evans, 2002; Hough and Elliot, 2004; Boatwright and Bundock, 2008a, 2008b; Hough and Hutton, 2008; Hough and Martin, 2018). These reinterpretations, combined with DYFI data for more recent events, will eventually produce a uniform shaking dataset with which earthquake hazard map performance can be assessed.

Probabilistic seismic hazard assessment maps show the amount of shaking a site is expected to experience in a given observation window, for an event with a given return period, with a certain probability. Maps of intensity observations have been used to assess earthquake hazard map performance in Japan, in Italy, and in the Central and Eastern United States (Stein et al., 2015; Brooks et al., 2016, Brooks et al., 2017). However, such testing has not been possible in California due to a lack of a long record of consistently interpreted intensity data. Further work will be needed to compile such a dataset for all moderate to large historic and early instrumental earthquakes in California. Further studies, informed by the discussion of uncertainties presented in this study, can also potentially improve magnitude estimates of key events.

9. Data and resources

The primary dataset of reports of shaking from the 1952 Kern County, CA earthquake and the historic intensity assignments are from: U.S. Department of Commerce, Environmental Services Administration, Coast and Geodetic Survey, 1966. Abstracts of earthquake reports for the Pacific Coast and the Western Mountain Region, MSA-74 April, June, July 1952.

The WWF surface trace used to approximate the midpoint of the surface rupture is from: U.S. Geological Survey (and California Geological Survey), 2006, Quaternary fault and fold database for the United States, from USGS web site: http://earthquake.usgs.gov/hazards/qfaults/, last accessed July 2017.

The major physiographic boundaries in Fig. 5 are from Fenneman, N.M., and Johnson, D.W, 1946, Physiographic divisions of the conterminous U. S.: https://water.usgs.gov/GIS/metadata/usgswrd/XML/physio.xml, last accessed July 2018.

The maps used to confirm location of historic addresses come from the USGS historical topographic map explorer website: http://historicalmaps.arcgis.com/usgs/, last accessed July 2017.

Latitude/longitude for cities listed in the primary dataset come from the NOAA Earthquake Intensity Database: https://www.ngdc.noaa.gov/hazard/intintro.shtml, last accessed February 2018.

Retroactively reported DYFI data for the 1952 Kern County earthquake can be found at: https://earthquake.usgs.gov/earthquakes/eventpage/ci3319401#dyfi DYFI data were downloaded from the USGS Web Site, http://earthquake.usgs.gov/earthquakes/dyfi/, last accessed February 2018.

Figs. 2–5 were generated using GMT software (Wessel and Smith, 1991).

Acknowledgements

Leah Salditch thanks the Northwestern Institute on Complex Systems – Data Science Initiative for funding her research. Edward Brooks thanks the Northwestern Institute for Policy Research for funding his research. The authors thank Emile Okal, John Ebel, Morgan Page, and one anonymous reviewer for helpful comments.

Declarations of interest

None.

References

Abe, K., 1981. Magnitudes of large shallow earthquakes from 1904 to 1980. Phys. Earth Plan. Int. 27 (1), 72–92.
Adhikari, S.R., Baysal, G., Dixit, A., Martin, S.S., Landes, M., Bossu, R., Hough, S.E., 2017. Towards a unified near-field intensity map of the 2015 Gorkha, Nepal, earthquake. Earthquake Spectra 33 (S1), S21–S34.
Ambraseys, N.N., 1971. Value of historical records of earthquakes. Nature 232, 375–379.
Ambraseys, N.N., et al., 1983. Notes on historical seismicity. Bull. Seismol. Soc. Am. 73 (6), 1917–1920.
Atkinson, G.M., Wald, D.J., 2007. "Did You Feel It?" intensity data: a surprisingly good measure of earthquake ground motion. Seismol. Res. Lett. 78 (3), 362–368.
Bakun, W.H., 2006. Estimating locations and magnitudes of earthquakes in Southern California. Bull. Seismol. Soc. Am. 96 (4A), 1278–1295.
Bakun, W.H., Wentworth, C.M., 1997. Estimating earthquake location and magnitude from seismic intensity data. Bull. Seismol. Soc. Am. 87 (6), 1502–1521.

Bawden, G.W., 2001. Source parameters for the 1952 Kern County earthquake, California: a joint inversion of leveling and triangulation observations. J. Geophys. Res. 106 (B1), 771–785.
Bawden, G.W., Donnellan, A., Kellogg, L.H., Dong, D., Rundle, J.B., 1997. Geodetic measurements of horizontal strain near the White Wolf fault, Kern County, California, 1926–1993. J. Geophys. Res. 102 (B3), 4957–4967.
Ben-Menahem, A., 1977. Renormalization of the magnitude scale. Phys. Earth Planet. Inter. 15, 315–340.
Boatwright, J., Bundock, H., 2008a. Modified mercalli intensity maps for the 1868 Hayward earthquake plotted in ShakeMap formt. USGS Open-File Report 2008-1121.
Boatwright, J., Bundock, H., 2008b. The distribution of modified mercalli intensity in the 18 April 1906 San Francisco earthquake. Bull. Seismol. Soc. Am. 98 (2), 890–900.
Borcherdt, R.D., 1970. Effects of local geology on ground motion near San Francisco Bay. Bull. Seismol. Soc. Am. 60 (1), 29–61.
Brooks, E.M., Stein, S., Spencer, B.D., 2016. Comparing the performance of Japan's earthquake hazard maps to uniform and randomized maps. Seismol. Res. Lett. 87 (1), 90–102.
Brooks, E.M., Stein, S., Spencer, B.D., Salditch, L., Petersen, M.D., McNamara, D.E., 2017. Assessing earthquake hazard map performance for natural and induced seismicity in the central and eastern United States. Seismol. Res. Lett. 89 (1), 118–126. https://doi.org/10.1785/0220170124.
Brune, J.N., Anooshehepoor, A., Shi, B., Zeng, Y., 2004. Precarious rock and overturned transformer evidence for ground shaking in the Ms 7.7 Kern County earthquake: an analog for disastrous shaking from a major thrust fault in the Los Angeles basin. Bull. Seismol. Soc. Am. 94 (6), 1993–2003.
Byerly, P., Dyk, H., 1936. The questionnaire program for collecting earthquake data, Earthquake Investigations in California, 1934-1935, Special Publication No. 201, U.S. Department of Commerce Coast and Geodetic Survey, Washington, DC, 43-48.
Dengler, L.A., Dewey, J.W., 1998. An intensity survey of households affected by the Northridge, California, earthquake of 17 January 1994. Bull. Seismol. Soc. Am. 88 (2), 441–462.
Dewey, J.W., Reagor, B.G., Dengler, L., Moley, K., 1995. Intensity distribution and isoseismal maps for the Northridge, California earthquake of January 17, 1994. USGS Open-File Report 95-92.
Foulger, G.R., Wilson, M.P., Gluyas, J.G., Julian, B.R., Davies, R.J., 2017. Global review of human-induced earthquakes. Earth-Sci. Rev. https://doi.org/10.1016/j.earscirev.2017.07.008.
Gutenberg, B., Richter, C.F., 1954. Seismicity of the Earth and associated phenomena, Second ed. Princeton University Press, Princeton, New Jersey.
Hearn, E.H., Pollitz, F.F., Thatcher, W.R., Onishi, C.T., 2013. How do “ghost transients” from past earthquakes affect GPS slip rate estimates on southern California faults? Geochem. Geophys. Geosyst. 14, 828–838. https://doi.org/10.1002/ggge.20080.
Hough, S.E., 2013. Spatial variability of ‘Did You Feel It?’ intensity data: insights into sampling biases in historical earthquake intensity distributions. Bull. Seismol. Soc. Am. 103 (5), 2767–2781. https://doi.org/10.1785/0120120285.
Hough, S.E., 2014. Earthquake intensity distributions: a new view. Bull. Earthq. Eng. 12, 135–155. https://doi.org/10.1007/s10518-013-9573-x.
Hough, S.E., Elliot, A., 2004. Revisiting the 23 February 1892 Laguna Salada earthquake. Bull. Seismol. Soc. Am. 94 (4), 1571–1578.
Hough, S.E., Hutton, K., 2008. Revisiting the 1872 Owens Valley, California. Earthquake Bull. Seismol. Soc. Am. 98 (2), 931–949.
Hough, S.E., Page, M., 2011. Toward a consistent model for strain accrual and release for the New Madrid Seismic Zone, central United States. J. Geophys. Res. 116, B03311. https://doi.org/10.1029/2010JB007783.
Hough, S.E., Tsai, V.C., Walker, R., 2017. Was the Mw 7.5 1952 Kern County, California, earthquake induced (or triggered)? J. Seismol. 21, 1613–1621. https://doi.org/10.1007/s10950-017-9685-x.
Hough, S.E., Martin, S.S., 2018. A proposed rupture scenario for the 1925 Mw6.6 Santa Barbara, California, earthquake, in review.
Huo, J.-R., Hwang, H.H.M., 1995. Seismic fragility analysis of equipment and structures in a Memphis electric substation. National Center for Earthquake Engineering Research, Technical Report NCEER-95-0014.
Hutton, K., Woessner, J., Hauksson, E., 2010. Earthquake monitoring in southern California for seventy-seven years (1932–2008). Bull. Seismol. Soc. Am. 100 (2), 423–446. https://doi.org/10.1785/0120090130.
Kanamori, H., Jennings, P.C., 1978. Determination of local magnitude, M_L, from strong-motion accelerograms. Bull. Seismol. Soc. Am. 68 (2), 471–485.
Martindale, D., Evans J.P., 2002. Historigraphical analysis of the 1857 Ft. Tejon earthquake, San Andreas Fault, California: Preliminary results, AGU Fall Meeting Abstracts, S12C-05.
Meltzner, A.J., Wald, D.J., 1999. Foreshocks and aftershocks of the great 1857 California earthquake. Bull. Seismol. Soc. Am. 89 (4), 1109–1120.
Murphy, L.M., Cloud, W.K., 1954. United States Earthquakes 1952, Department of Commerce, United States Government Printing Office, 117, Washington DC.
Musson, R.M., Grünthal, G., Stucchi, M., 2010. The comparison of macroseismic intensity scales. J. Seismol. 14 (2), 413–428.
Oakshotte, G.B., ed., 1955. Earthquakes in Kern County California during 1952. California Div. of Mines Bull, 171.
Peers, G.A., 1955. Damage to electrical equipment caused by Arvin-Tehachapi earthquake. Earthquakes in Kern County California during 1952. California Div. Mines Bull. 171.
Richter, C.F., 1958. Elementary Seismology. W.F. Freeman and Company, San Francisco Bailey Bros. & Swinfen Ltd., London.
Shao, J., Tu, D., 1995. The Jackknife and Bootstrap. Springer, New York.
Stein, R.S., Thatcher, W., 1981. Seismic and aseismic deformation associated with the 1952 Kern County, California, earthquake and relationship to the quaternary history of the White Wolf fault. J. Geophys. Res. 86 (B6), 4913–4928.
Stein, S., Spencer, B.D., Brooks, E.M., 2015. Metrics for assessing earthquake hazard map performance. Bull. Seismol. Soc. Am. 105 (4), 2160–2173.
Steinbrugge, K.V., Moran, D.F., 1954. An engineering study of the Southern California earthquake of July 21, 1952 and its aftershocks. Bull. Seismol. Soc. Am. 44 (2B), 201–462.
Trifunac, M.D., 2003. Nonlinear soil response as a natural passive isolation mechanism: the 1933 Long Beach, California earthquake. Soil. Dyn. Earthq. Eng. 23, 549–562.
U.S. Department of Commerce, Environmental Services Administration, Coast and Geodetic Survey, 1966. Abstracts of earthquake reports for the Pacific Coast and the Western Mountain Region, MSA-74 April, June, July 1952.
Wald, D.J., Dengler, L., Dewey, J.W., 1999a. Utilization of the internet for rapid community intensity maps. Seismol. Res. Lett. 70 (6), 680–693.
Wald, D.J., Quitoriano, V., Heaton, T.H., Kanamori, H., Scrivner, C.W., Worden, C.B., 1999b. TriNet “ShakeMaps”: rapid generation of peak ground-motion and intensity maps for earthquakes in Southern California. Earthq. Spectra 15 (3), 537–556.
Walls, C., Rockwell, T., Mueller, K., Bock, Y., Williams, S., Pfanner, J., Dolan, J., Fang, P., 1998. Escape tectonics in the Los Angeles metropolitan region and implications for seismic risk. Nature 394 (6691), 356.
Wessel, P., Smith, W.H.F., 1991. Free software helps map and display data. Eos Trans Am. Geophys. Union 72, 441.
Wood, H.O., Neumann, F., 1931. Modified Mercalli intensity scale of 1931. Bull. Seismol. Soc. Am. 21 (4), 277–283.
Worden, C.B., Gerstenberger, M.C., Rhoades, D.A., Wald, D.J., 2012. Probabilistic relationships between ground-motion parameters and modified Mercalli intensity in California. Bull. Seismol. Soc. Am. 102, 204–221. https://doi.org/10.1785/0120110156.
Working Group on California Earthquake Probabilities (WGCEP), 2008. The Uniform California Earthquake Rupture Forecast, Version 2 (UCERF 2): U.S.G.S. Open-File Report 2007-1437 and California Geological Survey Special Report 203 http://pubs.usgs.gov/of/2007/1437/.